ULTRASONIC IMAGING 15, 335-351 (1993)

QUANTITATIVE ULTRASOUND IMAGING: *IN VIVO* RESULTS IN NORMAL LIVER

J.A. Zagzebski, Z.F. Lu and L.X. Yao[1]

Department of Medical Physics
University of Wisconsin
Madison, WI 53706

A method for quantitative imaging of ultrasonic backscatter levels has been implemented on a clinical imager. The method is based on comparing echo signal data from a sample or patient to echo data processed in the same way but acquired from a reference phantom. The attenuation coefficient and the backscatter coefficient of the reference phantom are known, permitting these quantities to be estimated for the sample. In the present paper, the spatial location of echo data acquisition is retained in the backscatter data analysis; quantitative "backscatter estimator" images are constructed, from which the backscatter coefficient over a region of interest may be obtained. When applied to human liver images, backscatter coefficients determined in 10 normal subjects were in approximate agreement with *in vitro* liver backscatter coefficients reported by previous workers.

Key words: Attenuation coefficient; backscatter coefficient; liver; quantitative imaging; tissue phantoms; ultrasound.

I. INTRODUCTION

Current clinical ultrasound B-mode scanners produce high resolution, gray-scale images depicting relative ultrasound attenuation and backscatter levels in soft tissue. These images are operator, instrument and transmission-path dependent, thereby yielding only qualitative or at best semiquantitative information on ultrasonic scattering properties of tissues. Interest in more precisely quantitating ultrasonic scattering in tissues stems from evidence that a tissue's scattering properties are altered from normal in some disease conditions, for example, in diffuse liver disease [1 – 3]. Although present clinical ultrasound equipment allows detection of advanced diffuse disease if accompanied by variations in scattering and/or attenuation, the sensitivity to diffuse changes appears to be more limited for early stage disease [4].

---

[1]Current address: Siemens Quantum, Inc., Issaquah, WA.

0161-7346/93 $5.00

We are developing methods for quantitative ultrasound imaging of acoustic backscatter levels. The methods account for effects of the transducer beam, operator gain settings, instrument transfer functions and the acoustic propagation path on the amplitudes of echo signals. Quantitative backscatter imaging was investigated previously by O'Donnell [7] and later by our group [8, 9]. Such quantitative images, either in the form of frequency dependent "backscatter estimators" (see below) or locally averaged backscatter coefficients [9] might be more sensitive than current techniques, particulary for detection of early disease and for monitoring changes due to therapy [5 – 7]. The purpose of this paper is to outline this quantitative imaging method as it currently is implemented on a clinical ultrasound imager and to present initial results of acoustic backscatter coefficients in liver *in vivo* measured from quantitative images.

In previous reports [8, 9], instrument independent quantitative ultrasound images were formed using an absolute data reduction method employing a planar reflector as a reference. Quantitative ultrasound images described here are constructed using a reference phantom data reduction method [10], which simplifies calibrations and computational requirements. The essential elements of that method are outlined in this paper, and formulations that apply to quantitative backscatter imaging are introduced. The approach is similar to that described by Rhyne [11], differing in that signals from a standard clinical imager are used, and calibrations involve comparisons between signals from the imaged region and signals from the reference phantom rather than applying a reference planar reflector to normalize echo data. Other authors using a reference phantom to quantify acoustic properties of tissue include Meyer et al. [12], Nicolas [13] and Wilson et al.[14].

II. THEORY

A. Backscatter Coefficient for a Sample Volume

Figure 1 illustrates the quantitative backscatter imaging configuration. The pulsed beam from an ultrasound transducer is swept over a sample. For each position of the transducer, specified by beam line m and scanning plane n, an echo signal wavetrain is recorded. When the scatterers are randomly distributed, the backscattered echo voltage at time t following the emission of the pulse can be represented as [15]

$$v_s(t;m,n) = \int_{-\infty}^{\infty} d\omega T(\omega) B_o(\omega) e^{-i\omega t} \int\int\int_{\Omega} d\mathrm{r} N(\mathrm{r}) \Psi(\omega) [A_o(\mathrm{r},\omega)]^2, \qquad (1)$$

where $T(\omega)$ is a transfer function relating the force on the transducer at frequency ω to the signal voltage; $B_o(\omega)$ is a complex superposition coefficient which determines the form of the pressure pulse in the medium; $N(\mathrm{r})$ is the number density of scatterers in the vicinity of r; $\Psi(\omega)$ is the value of the angular distribution factor [16] for the scattered wave at 180°; $A_o(\mathrm{r},\omega)$ is proportional to the Rayleigh integral [17] for the case of uniform insonation of the transducer; and the volume, Ω includes all scatterers which can contribute significantly to the signal at time t. If $\bar{N}$ is the average number of discrete scatterers in a uniform volume element of the sample, the backscatter coefficient of this element is taken as $\eta(\omega) = \bar{N}\Psi^*(\omega)\Psi(\omega)$. Although this expression

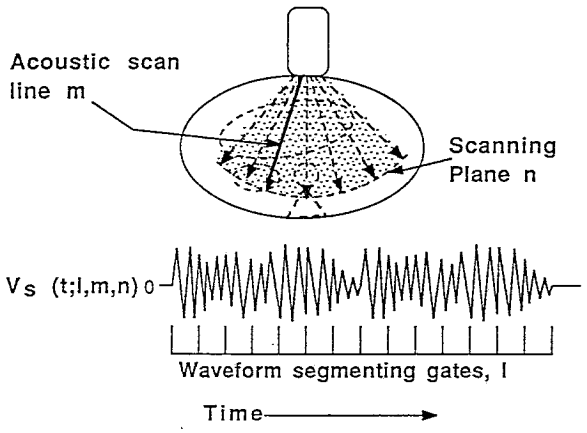

Fig. 1 Backscatter imaging arrangement. The labels ℓ, m and n are used to signify echo voltage data from the ℓ^{th} segment of scan line m in plane n.

implies a single scatterer size and type, it can be generalized to include sets of scatterers, each set having different properties, or a volume containing continuously varying inhomogeneities in density and compressibility.

During data analysis, this wavetrain is divided into contiguous segments, each segment identified with index ℓ. The backscatter coefficient at frequency ω_o, $\eta(\omega_o)$, is obtained by taking an ensemble average of the squared modulus of the Fourier transform of the echo signal voltage from the sample, and multiplying by factors which account for sound beam attenuation, transducer diffraction, properties of the transmitting medium and other instrumentation parameters as indicated in Eq. (1). If the sample has uniform acoustic properties (as is the case of reference phantoms used in this work) and if an ensemble average is obtained by averaging data from segment ℓ over all scan lines and scanning planes, the backscatter coefficient is [8, 15]

$$\eta(\omega_o) = \frac{\overline{V^*(\omega_o,\ell)V(\omega_o,\ell)}}{a_\ell(\omega_o)}, \tag{2}$$

where $\overline{V^*(\omega_o,\ell)V(\omega_o,\ell)}$ is also called the voltage spectral density function [26] of the echo signal (in units of $v^2 s$ per unit of bandwidth) and

$$a_\ell(\omega_o) = \int\int\int_{\Omega_\ell} d\mathbf{r} \left| \int_{-\infty}^{\infty} d\omega T(\omega) B_o(\omega) \frac{g(\omega)}{g(\omega_o)} W(\omega-\omega_o)[A_o(\mathbf{r},\omega)]^2 \right|^2 \tag{3}$$

Here, $g(\omega)$ represents the frequency dependence of the backscatter coefficient, $g(\omega_o)$ is the value of this function at the analysis frequency and $W(\omega-\omega_o)$ represents a windowing function used to select the ℓ^{th} segment in each beam line.

B. Separating Terms in the Expression for $a_\ell(\omega_o)$

In the reference phantom method, ratios of $\overline{V^*(\omega_o,\ell)V(\omega_o,\ell)}$ in the subject to the same quantity obtained from a well-characterized phantom are used to estimate the attenuation coefficient and the backscatter coefficient within a region in the subject. The method implies that the denominator of Eq. (2) can be factored into the product of separate terms, one that depends only on the medium and a second that depends only on the instrument and transducer. Define $I(\omega_o,\ell) \equiv \overline{V^*(\omega_o,\ell)V(\omega_o,\ell)}$. Rewriting Eq. (2), we have

$$I(\omega_o,\ell) = \eta(\omega_o)a_\ell(\omega_o) \tag{4}$$

Regarding the terms contributing to $a_\ell(\omega_o)$, the quantity $A_o(\mathrm{r},\omega)$ involves an integral that depends both on the ultrasound attenuation coefficient in the medium and on the size and shape of the transducer. Yao [18] has shown that the attenuation coefficient can be removed from the integral expression for $A_o(\mathrm{r},\omega)$, with no loss of accuracy as long as the transducer-to-field point distance is at least equal to the transducer diameter. Thus, for a uniform medium

$$A_o(\mathrm{r},\omega) \doteq e^{-\alpha(\omega)z}\int\int_S ds'' \frac{e^{i\frac{\omega}{c}|\mathrm{r}-\mathrm{r}''|}}{|\mathrm{r}-\mathrm{r}''|}, \tag{5}$$

where z is the axial distance from the transducer to the field point, $\alpha(\omega)$ and c are the attenuation coefficient and speed of sound in the medium and r'' points to area element ds'' on the transducer surface, S.

If the bandwidth of the system is narrow enough and the backscatter coefficient does not change rapidly with frequency, we can set the ratio $g(\omega)/g(\omega_o)$ to 1 in Eq. (3); we also can use the value of the attenuation coefficient at the center frequency of the pulse for the whole band. The echo signal voltage spectral density function from segment ℓ can then be written as

$$I(\omega_o,\ell) = \eta(\omega_o)e^{-4\alpha(\omega_o)z}\int\int\int_\Omega d\mathrm{r}' G^*(\mathrm{r}',\omega_o,t)G(\mathrm{r}',\omega_o,t), \tag{6}$$

where $G(\mathrm{r}',\omega_o,t)$ includes the factors $T(\omega)B_o(\omega)$, the window function and the integral in Eq. (5), and $z = \Delta z \times \ell$ where Δz corresponds to the axial distance between segments. Thus, $I(\omega_o,\ell)$ is written as the product of terms which depend on the medium and a term that depends on the transducer, instrument and signal processing.

C. Quantitative Backscatter Images

Individual measures of the squared modulus of the Fourier transform of the echo signal, $i(\omega_o;\ell,m,n)$, exhibit point-to-point statistical fluctuations because of wave interference when random media, such as tissues are interrogated. The term "backscatter estimator" [8], $BSE(\omega_o;\ell,m,n)$, is used to express the tissue scattering for these individual measures. Backscatter estimators are individual samples of the backscattered signal, corrected for attenuation and instrumentation dependencies. When averaged over a region, the estimators yield the backscatter coefficient of that region. Using this

notation, we have for $i(\omega_o;\ell,m,n)$,

$$i(\omega_o;\ell,m,n) = BSE(\omega_o;\ell,m,n)e^{-4\int_0^z \alpha(\omega_o;z',m,n)dz'} \int\int\int_\Omega d\mathrm{r}' G^*(\mathrm{r}',\omega_o,t)G(\mathrm{r}',\omega_o,t), \tag{7}$$

where z' refers to the depth along scan line m in plane n and the exponential attenuation factor now includes the possibility that attenuation is not uniform over the scanned volume.

Let $ri(\omega_o;\ell,m,n)$ be the ratio of the squared modulus of the Fourier transform of the echo signal corresponding to location (ℓ,m,n) in the test sample to the value of the echo signal voltage spectral density at ω_o, from locations centered at depth $z = \Delta z \times \ell$ in the reference phantom. Then

$$ri(\omega_o;\ell,m,n) \equiv \frac{i(\omega_o;\ell,m,n)}{I_{ref}(\omega_o;\ell)} = \frac{BSE(\omega_o;\ell,m,n)e^{-4\int_0^z \Delta\alpha(\omega_o;z',m,n)dz'}}{\eta_{ref}(\omega_o)} \tag{8}$$

where the subscript "ref" denotes the reference phantom and $\Delta\alpha$ is the *difference* between the attenuation coefficient in the sample at the location specified and the attenuation coefficient in the reference phantom. (The speed of sound has been assumed to be the same in both media.) Notice that the expression for $ri(\omega_o;\ell,m,n)$ does not contain transducer or instrumentation dependencies, but only depends on the properties of the sample and the reference phantom.

If the $\Delta\alpha(\omega_o;z',m,n)$ are known, or once they have been estimated (see next section), backscatter estimator images may be constructed using

$$BSE(\omega_o;\ell,m,n) = ri(\omega_o;\ell,m,n)\eta_{ref}(\omega_o)e^{4\int_o^z \Delta\alpha(\omega_o;z',m,n)dz'} \tag{9}$$

These images represent *absolute scattering levels* of the sample. They are analogous to conventional B-mode images, except they have been corrected for attenuation and most instrumentation effects, and absolute calibrations have been applied. To the extent that the statistical fluctuations in image brightness depend on the system, these images do exhibit instrumentation dependencies. However, they can be used to measure the backscatter coefficient as a function of frequency by averaging estimators over a selected region of interest.

D. Estimating the Attenuation Coefficient in a Region of Interest

In general, it is necessary first to measure the ultrasound attenuation coefficient in order to produce quantitative backscatter images. This may be done for regions where both the backscatter coefficient and the attenuation coefficient are uniform; ie, these quantities do not vary across beam lines or between scanning planes within this region. Let us define $RI(\omega_o;\ell)$ as the average $ri(\omega_o;\ell,m,n)$ for a uniform region of interest. Substituting this into Eq. (8) and taking the logarithms of both sides yields

$$\ln[\mathrm{RI}(\omega_o;\ell)] = \ln\left[\frac{\eta_x(\omega_o)}{\eta_{\mathrm{ref}}(\omega_o)}\right] - 4\int_0^z \Delta\alpha(\omega_o;z')\mathrm{d}z' \tag{10}$$

where η_r is the backscatter coefficient within the region of interest. If this region is in the depth interval $z_1 \leq z \leq z_2$, and if the difference between its attenuation and that of the reference phantom is $\Delta\alpha_r(\omega_o)$, we have for the attenuation part of the righthand term

$$-4\int_0^z \Delta\alpha(\omega_o; z', m, n)dz' = -4\int_0^{z_1} \Delta\alpha(\omega_o; z', m, n)dz' - 4\Delta\alpha_r(\omega_o)(z - z_1) \qquad (11)$$

The first term on the right in Eq. (11) involves the tissue/sample path between the transducer and the region of interest, while the second term represents attenuation between z_1 and z. For this region, a least squares analysis is used to fit the function $\ln[\mathrm{RI}(\omega_o; \ell)]$ vs depth to a straight line. The slope of this line yields $\Delta\alpha_r(\omega_o)$ and, hence, the attenuation coefficient in the region of interest.

Generally, the attenuation coefficient can be estimated in this way only for fairly large, uniform sample volumes [25]. When scanning intact anatomical structures, such as the liver, a particularly important problem involves attenuation within the body wall, represented by the first term on the right in Eq. (11). At present, we are able only to provide estimates of body wall attenuation using ultrasound based measurements of tissue layer thicknesses and assuming values for the attenuation coefficient that have been published in the literature. This approach is discussed in more detail in section III.

III. EXPERIMENTAL METHODS

A. Data Acquisition

Figure 2 shows the experimental apparatus used in this study. A Siemen's Sonoline SL-1 mechanical sector scanner equipped with 3.5, 5 and 7.5 MHz transducer assemblies was used to acquire echo data. The scanner was modified by the manufacturer to

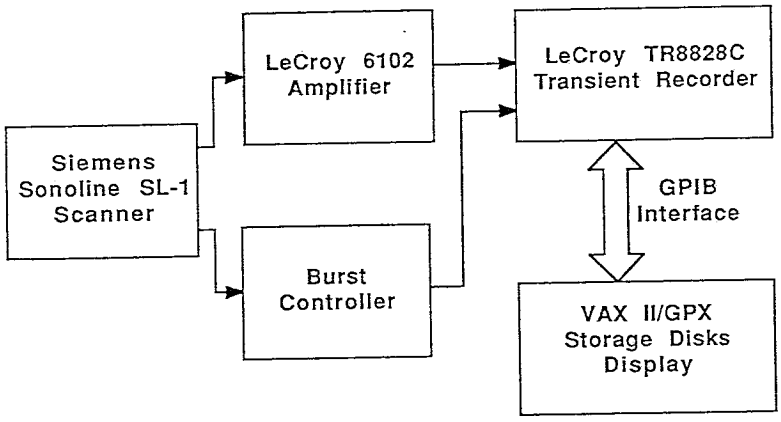

Fig. 2 Apparatus used to record echo data from subjects.

enable acquisition of rf echo signals following depth dependent amplification, but before demodulation. Timing signals, including the start of each scan line and the start of each scan plane sequence, also were provided by the manufacturer. These were used, along with a "burst control" circuit, to select an area within the subject from which echo data were acquired. Echo signals were digitized at 50 MHz in a LeCroy TR8828C Transient recorder equipped with 768 kbytes memory. Data were stored on the disk of a microVax computer for analysis.

Ten individuals ranging in age from 15 to 54, all believed to have normal livers, were used as subjects. Each subject was scanned while in the supine position; the system output was maximized and the gain and TGC settings of the scanner were adjusted to produce a uniform image of the liver using a subcostal window. Four scans of the right lobe of the liver were made in closely spaced parallel planes with the 3.5 MHz handheld probe. Each scan consisted of 110 lines of rf signals. The recorded signals began 40 μs after the transducer excitation pulse and the length of digitized signal segments was 140 μs.

Following rf data acquisition in the patient, echo signals also were recorded from a large reference phantom, using the same transducer, output power, gain and TGC settings. Signals from 6 scan planes, each including 50 beam lines were obtained. The attenuation coefficient of the reference phantom is 0.52 dB/cm/MHz and the backscatter coefficient is 0.0006 $cm^{-1}sr^{-1}$ at 3 MHz. These parameters were used in Eq. (9) to construct quantitative BSE images of the patient.

After data acquisition, subjects were scanned with a 7.5 MHz transducer in order to image the superficial tissue region in the vicinity of the scanned volume. The transducer orientation was the same as that used in the data acquisition phase, and an attempt was made to apply the same pressure on the body wall as was used in the rf echo data acquisition. Since the tip of the 7.5 MHz probe was of nearly the same geometry as the 3.5 MHz transducer, it was assumed that the body wall was distorted the same degree in both scans. A small field of view, high magnification image was recorded with the 7.5 MHz probe. This was then used to estimate the amount of body wall fat and muscle in the scanning plane.

B. Signal Processing

During analysis, the time dependent echo signal is split into two channels, multiplied by orthogonal waves with frequency ω_o and convolved with a 3-term Blackman-Harris window [19] which serves as a low-pass filter. The echo voltages from each channel are then squared and added, yielding the $i(\omega_o; \ell, m, n)$ data at the analysis frequency. This procedure is repeated for each of 7 analysis frequencies spanning the frequency bandwidth of the transducer. All processing is done in software using routines written in Fortran.

The low-pass filter p(t) in the signal processing is expressed as

$$p(t) = a_o - a_1 cos(bt) + a_2 cos(2bt). \tag{12}$$

Here $b = 2\pi/\tau$, where τ is the duration of the time window, $a_o = 0.42323$, $a_1 = 0.49755$,

and $a_2 = 0.07922$. The spectrum of this window, $P(\omega)$, has very low side lobes, the highest being 67 dB below the main lobe [19].

The duration of the window determines the width of the frequency band of the low-pass filter used to obtain $i(\omega_o; \ell, m, n)$ from the broad-band echo signal. In applications using a broad bandwidth pulse from a clinical transducer, the resultant spectral density of the filtered signal is the product of the spectral density function of the echo signal and the filtering function of the bandpass filters. The average frequency of the filtered echo voltage spectrum tends to shift towards the frequency at which the spectral density of the echo signal has the greatest value. Thus, a narrow frequency bandwidth is desired to guarantee a small frequency shift. However, this also means a long duration time window, which deteriorates the axial resolution.

To find an optimal window size [18], rf echo data from two phantoms were acquired using both the 5 MHz and 3.5MHz center frequency transducers. The phantoms have the same backscatter coefficient, but differ in that one has tissue-like attenuation (0.44 dB/cm/MHz +0.0198 dB/cm/MHz^2) while the other has significantly lower attenuation (0.1405 dB/cm/MHz + 0.0252 dB/cm/MHz^2). Echo signals were analyzed at frequencies of 2.5, 3, 3.5, 4.5, 5 and 5.5 MHz, computing $RI(\omega_o, \ell)$, ratios of the echo voltage spectral density from the two phantoms. The outcomes are affected by the window durations, as shown in figure 3 where the duration ranges from 0.25 μs to 32 μs.

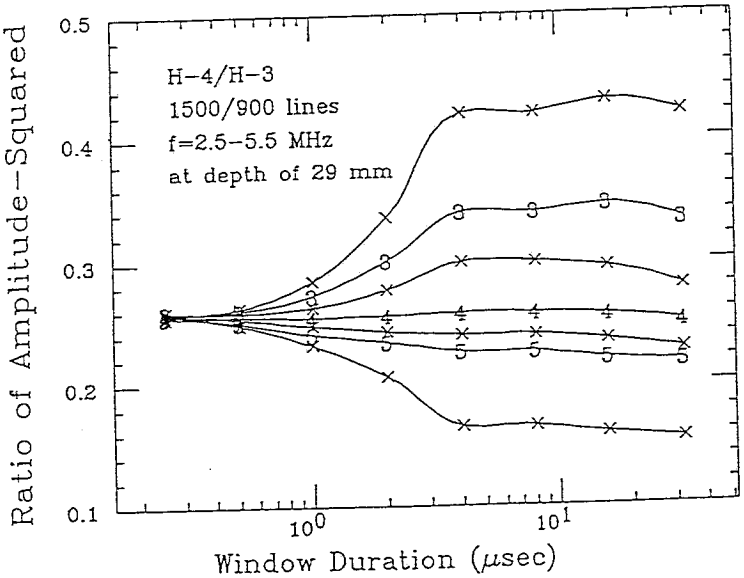

Fig. 3 The ratio of the value of the voltage spectral density function, $RI(\omega_o, \ell)$ in two different phantoms, vs. the duration of the Blackman-Harris window used to select signals from the depth of interest. The ratio is shown for analysis frequencies ranging from 2.5 MHz (top curve) to 5.5 MHz (bottom). Stable results are obtained when the window duration is at least 4 μs.

In figure 3, each curve represents data at a fixed depth for a different analysis frequency, the top curve being for 2.5 MHz and the bottom for 5.5 MHz. Notice that for very short duration time windows, ratios of the echo voltage spectral density from the two phantoms are essentially independent of analysis frequency; that is, the spectral bandwidth of the Blackman-Harris window provides no selection of frequency dependent echo data. However, for window durations of 4 μs and greater, results appear to be stable. Therefore, frequency shift errors are minimized by keeping the window duration longer than 4 μs. To optimize the axial resolution as well as to minimize the frequency shift error, we used a 4-μs time window in the data analysis for the present study.

IV. RESULTS

The 3.5 MHz center frequency echo data from the liver of each subject were analyzed at frequencies of 2.25, 2.50, 2.75, 3.0, 3.25, 3.5 and 3.75 MHz. The interval between the centers of successive data segments was 0.64 μs, corresponding to about a 0.5 mm axial distance. Data from each scan from the liver were analyzed individually to obtain $i(\omega_o; \ell, m, n)$ for each frequency and each data point. Corresponding data for all 300 acoustic lines from the reference phantom were averaged at each depth to form $I_{ref}(\omega_o, \ell)$ for each frequency.

$ri(\omega_o; \ell, m, n)$, the ratio of the amplitude-squared echo at frequency ω_o from location (ℓ, m, n) in a subject's liver to the average amplitude-squared from depth segment ℓ in the reference, was then computed for each of the four scans and converted into images. An example is shown in figure 4. This *ratio* image set depicts one scanning plane, showing the liver and kidney of a 46 year old male subject. Each image in this set corresponds to a separate analysis frequency, ranging from 2.25 MHz in the upper left to 3.75 MHz in the second image from the lower right. The lower right image is a broadband image, obtained by envelope-detecting the original unfiltered echo data, where a Hilbert transform was used for demodulation. Notice that at low frequencies, the average brightness in these *ratio* images appears greater than it does at higher frequencies. This reflects the different frequency dependence of scattering in the reference phantom compared to the frequency dependence of scattering in the subject's liver. Over the frequency range included in this analysis, backscatter in the reference phantom, which contains 60.5 μm diameter, glass-bead scatterers, increases with increasing frequency at a greater rate than the backscatter coefficient of liver.

These images were used to facilitate estimates of $\Delta\alpha_r(\omega_o)$ and hence, attenuation coefficients for the liver using the methods following Eq. (11). For each image, a region of interest was selected within the liver where there were no large vessels or interfaces. The size of the region of interest was chosen as large as possible to diminish statistical uncertainties [25]. $ri(\omega_0; l, m, n)$ were averaged over acoustic lines within the region of interest. The resultant $RI(\omega_0; l)$ vs. depth was then fit to a straight line by least squares analysis, yielding the slope for calculating the difference between the attenuation coefficient in the region of interest and in the reference phantom. Generally, such a region of interest includes 25 - 30 acoustic lines and extends 5 cm axially in

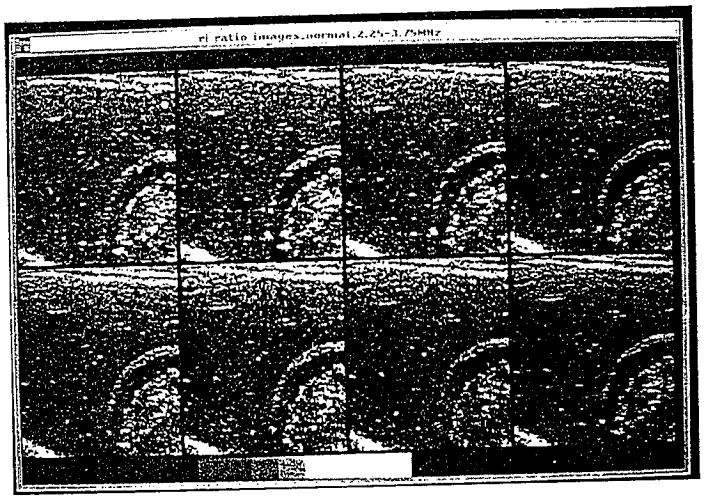

Fig. 4 A set of $ri(\omega_o; \ell, m, n)$ images from one scanning plane of one subject in this study. The longitudinal scanning plane was through the upper abdomen, depicting the liver, diaphragm and right kidney. The set represents image data at frequencies, ranging from 2.25 MHz (top left) to 3.75 MHz (second from lower right); the lower right image is broadband, obtained by envelope-detecting the echo signals from the subject and the signals from the reference phantom.

each scanning plane. The attenuation coefficient difference was measured in this way from 4 parallel scanning planes. The results were then averaged and corrected with the attenuation coefficient of the reference phantom to provide the attenuation coefficient of the liver.

Table 1 presents the attenuation coefficient vs. frequency for all 10 subjects. Values in parentheses are the standard deviations for individual frequency components for each subject. Results are very close to 0.53 dB/cm/MHz, agreeing with other researchers estimates of attenuation in normal liver [20].

Backscatter estimators were computed for each image plane after correcting for the measured attenuation in the liver and the *estimated* attenuation in the body wall. The latter was done in a fashion similar to that described earlier [21] where the 7.5 MHz body wall image was used to obtain distances to apply to the simple model outlined in figure 5. Superficial layers in the 7.5 MHz B-mode image were taken as fat and an intervening layer between fat and liver was assumed to be muscle. 0.6 dB/cm/MHz and 1.3 dB/cm/MHz were used as values for the attenuation coefficient slope in fat and muscle, respectively [22].

Quantitative backscatter estimator images corresponding to the same plane shown in figure 4 are presented in figure 6. The eight images in this set correspond to analysis frequencies ranging from 2.25 MHz (upper left) to 3.75 MHz (second image from the

Table 1. Attenuation coefficient in the liver for each subject

Attenuation Coefficient in dB/cm (Standard Deviation in dB/cm)							
Subject	2.25 MHz	2.50 MHz	2.75 MHz	3.0 MHz	3.25 MHz	3.5 MHz	3.75 MHz
1	1.13 (0.052)	1.26 (0.076)	1.36 (0.048)	1.43 (0.064)	1.56 (0.084)	1.72 (0.112)	1.93 (0.105)
2	1.13 (0.051)	1.23 (0.065)	1.29 (0.07)	1.50 (0.08)	1.65 (0.048)	1.77 (0.065)	1.95 (0.071)
3	1.48 (0.028)	1.62 (0.013)	1.75 (0.074)	1.81 (0.081)	1.88 (0.099)	2.0 (0.139)	2.11 (0.119)
4	1.36 (0.106)	1.48 (0.108)	1.63 (0.102)	1.77 (0.114)	1.9 (0.107)	2.08 (0.12)	2.24 (0.116)
5	1.07 (0.177)	1.27 (0.170)	1.41 (0.194)	1.52 (0.172)	1.67 (0.150)	1.83 (0.154)	1.91 (0.143)
6	1.02 (0.041)	1.05 (0.033)	1.24 (0.069)	1.33 (0.056)	1.42 (0.067)	1.53 (0.071)	1.66 (0.074)
7	1.39 (0.053)	1.51 (0.048)	1.59 (0.068)	1.62 (0.1)	1.73 (0.171)	1.84 (0.215)	2.04 (0.193)
8	1.26 (0.081)	1.34 (0.064)	1.56 (0.053)	1.65 (0.082)	1.76 (0.045)	1.99 (0.129)	2.17 (0.087)
9	1.44 (0.079)	1.57 (0.070)	1.72 (0.070)	1.86 (0.057)	1.93 (0.095)	1.99 (0.129)	2.01 (0.103)
10	1.37 (0.03)	1.53 (0.036)	1.62 (0.051)	1.69 (0.037)	1.78 (0.059)	1.9 (0.077)	1.94 (0.087)
AVE.	1.26	1.39	1.52	1.62	1.73	1.87	2
AVE/Freq dB/cm-MHz	0.56	0.556	0.553	0.54	0.532	0.534	0.533

lower right). The broadband image in the lower right panel was obtained by correcting for attenuation losses and instrumental factors in the envelope-detected image. Notice that the scattering level in the parenchyma of the kidney is lower than that of the liver, especially at lower frequencies.

These images depict *absolute* scattering levels in the liver, kidney and surrounding tissues. The gray scale has been calibrated such that midgray represents 15 dB above a reference level of 1×10^{-4} $cm^{-1}sr^{-1}$ and the increment between gray bars is

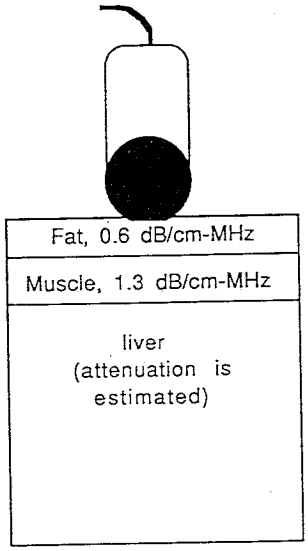

Fig. 5 Schematic illustration of model used to correct for losses in the body wall of the subject. The thicknesses of fat and muscle were estimated from B-mode images; the attenuation coefficients used to compensate for body wall attenuation are those shown.

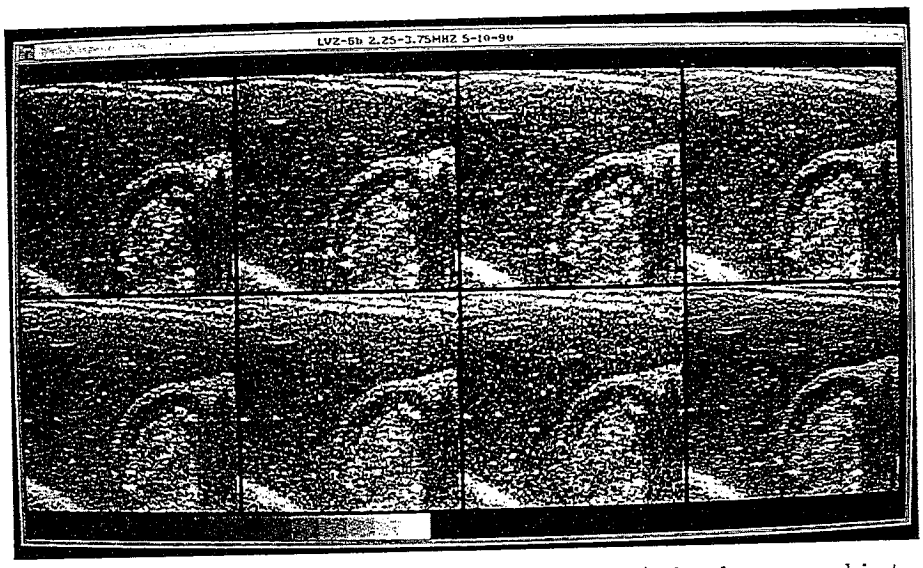

Fig. 6 Set of backscatter estimator images, $BSE(\omega_o; \ell, m, n)$, for the same subject and scanning plane as in figure 4. (See the caption of figure 4 for the frequencies corresponding to each image.) The gray scale is calibrated such that the midgray represents a backscatter level 15 dB greater than $1 \times 10^{-4}\text{cm}^{-1}\text{sr}^{-1}$.

4 dB. The frequency dependence of scattering over the bandwidth of the echo voltage spectrum can be appreciated from these images. Comparisons of the image brightness at the higher analysis frequencies with that at the lower analysis frequencies suggests that there is higher scattering at 3.75 MHz than at 2.25 MHz. Statistical fluctuations among these backscatter estimator images can be reduced by averaging, as shown in backscatter coefficient images generated using the absolute data reduction method [8,9].

Regions of interest were selected on the backscatter estimator images in the same way described above for the attenuation measurement. The backscatter estimators within the selected region of interest were averaged to provide the backscatter coefficient for that region. Results from the 4 parallel scanning planes were averaged to give the backscatter coefficient of the liver for each subject. Table 2 presents the results for all ten subjects. The subject number identifier in this table is the same as in table 1.

Figure 7 presents the average backscatter coefficient vs. frequency for all 10 subjects. The apparent increase in scattering with increasing frequency, seen in figure 6, is evident from the results in figure 7. The average backscatter coefficient at 2.25 MHz ($4.75 \times 10^{-4}\text{cm}^{-1}\text{sr}^{-1}$ agrees reasonably well with *in vivo* results at this frequency reported by O'Donnell [7]. For an ultrasound frequency of 2.25 MHz, he found an average backscatter coefficient of $3.5 \times 10^{-4}\text{cm}^{-1}\text{sr}^{-1}$ in 13 normal subjects, though he used a different estimation for body wall losses and processed envelope detected echo signals

Table 2. Backscatter coefficients in the liver for each subject

Backscatter Coefficient in $10^{-4}\text{cm}^{-1}\text{sr}^{-1}$							
Subject	2.25 MHz	2.50 MHz	2.75 MHz	3.0 MHz	3.25 MHz	3.5 MHz	3.75 MHz
1	1.91	2.36	3.1	3.59	3.70	3.85	3.95
2	1.93	2.43	3.21	3.74	4.27	5.09	5.86
3	6.63	7.56	8.85	9.5	9.75	9.7	9.77
4	2.55	3.4	4.54	5.4	6.15	7.28	8.4
5	3.35	4.44	6.09	6.89	7.59	8.42	9.4
6	4.22	5.01	5.57	6.06	6.75	7.3	7.44
7	6.56	7.24	7.76	8.69	9.65	9.8	9.76
8	3.62	4.37	5.02	5.34	5.77	6.26	6.51
9	6.88	7.33	7.93	7.96	7.9	8.71	11.4
10	9.84	9.99	10.02	10.39	10.40	10.22	11.46
AVE	4.75	5.41	6.21	6.76	7.19	7.69	8.4

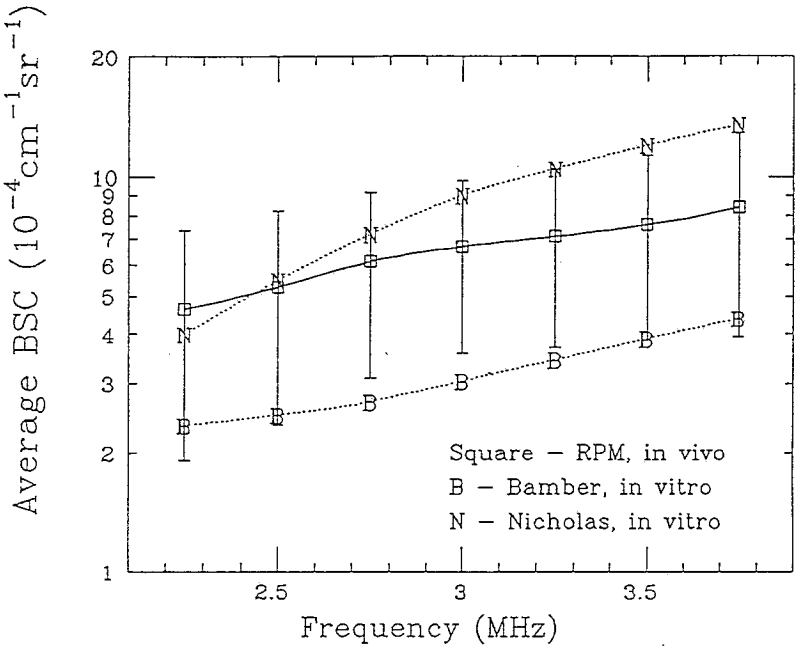

Fig. 7 Mean backscatter coefficients in the liver for 10 normal subjects, plotted vs ultrasound frequency. Error bars represent 1 standard deviation. Also shown are results for backscatter coefficients in normal liver obtained by Nicholas [23] (N) and Bamber [24] (B).

from the scan converter of a clinical ultrasound imager rather than rf echo signals as in this work. Also shown in this figure are backscatter coefficients obtained by Nicholas [23] and Bamber [24] for *in vitro* liver. The measured backscatter coefficients in the present study appear to be intermediate between those of these earlier workers, and the level of agreement with those workers' *in vitro* data is interesting.

V. SUMMARY

We have outlined methods for constructing quantitative ultrasound images related to the frequency dependent backscatter coefficient of tissue. The methods use data reduction techniques originally developed for measuring ultrasonic scattering properties of small samples, adapted for imaging. With present ultrasound equipment, a reference phantom method was found to be convenient to implement. The method yielded attenuation coefficients in normal liver that were in agreement with results of previous workers. New quantitative images of *in vivo* backscatter estimators were presented for individual frequencies throughout the bandwidth of the pulse. Backscatter coefficients

obtained from data in these images are in the range of those obtained for *in vitro* liver by previous workers.

Future work will explore the potential of these processing methods to differentiate normal from abnormal tissue and thus add to the diagnostic capability of medical ultrasound. Additional work also is necessary to refine methods for accounting for losses in the patient body wall, still a potentially high source of uncertainty of these measurements. If diagnostic capabilities are proven useful, the reference phantom method as described in this paper could easily be adopted to real time echo data acquisition and display.

VI. ACKNOWLEDGMENTS

The authors are grateful to Kathryn McSherry and Colleen Schutz for assistance in preparing the manuscript. This work was supported in part by NIH grant RO1 CA39224.

REFERENCES

[1] Holm, H., Kristensen, J., Rasmussen, S., Pedersen, J., Hancke, S., Jensen, F., Gammelgaard, J. and Smith, E., *Abdominal Ultrasound Static and Dynamic Scanning, 2nd edition*, pp. 96-97 (Munksgard, Copenhagen, 1980.).

[2] Garra, B.S., Insana, M.F., Shawker, T.H., Wagner, R.F., Bradford, M. and Russell, M.A., Quantitative ultrasonic detection and classification of diffuse liver disease; comparison with human performance, *Investigative Radiology 24,* 196-203 (1989).

[3] Garra, B.S., Insana, M.F., Shawker, T.H. and Russell, M.A. Quantitative estimation of liver attenuation and echogenicity: normal state versus diffuse liver disease, *Radiology 162,* 61-67 (1987).

[4] Sandford, N.L., Walsh, P., Matis, C., Baddeley, H. and Powell, L.W., Is utrasonography useful in the assessment of diffuse parenchymal disease? *Gastroenterology 89,* 186-191 (1985).

[5] Campbell, J. A. and Waag, R. C., Measurements of calf liver ultrasonic differential and total scattering cross-sections, *J. Acoust. Soc. Am. 75,* 603-611 (1984).

[6] Lizzi, F.L., King, D.L., Rorke, M.C., Hui, J., Ostromogilsky, M., Yaremko, M.M., Feleppa, E.J. and Wai, P., Comparison of theoretical scattering results and ultrasonic data from clinical liver examinations, *Ultrasound Med. Biol. 14,* 377-385 (1988).

[7] O'Donnell, M. and Reilly, H.F., Clinical evaluation of the B'-scan, *IEEE Trans. Sonics Ultrason. SU-32,* 450-457 (1985).

[8] Boote, E., Zagzebski, J., Madsen, E., and Hall, T. Instrument independent backscatter coefficient imaging, *Ultrasonic Imaging 10*, 121-138 (1988).

[9] Boote, E., Hall, T., Madsen, E. and Zagzebski, J., Improved resolution backscatter coefficient imaging, *Ultrasonic Imaging 13,* 347-359 (1991).

[10] Yao, L., Zagzebski, J. and Madsen, E., Backscatter coefficient measurements using a reference phantom to extract depth-dependent instrumentation factors, *Ultrasonic Imaging 12,* 58-70 (1990).

[11] Rhyne, T.L. and Sagar, K.B., IBR5: An optimal measurement of integrated backscatter and cyclic variation of integrated backscatter, *Ultrasonic Imaging 12,* 189-204 (1990).

[12] Meyer, C., Herron, D., Carson, P., Banjavic, R., Thieme, G., Bookstein, F. and Johnson, M., Estimation of ultrasonic attenuation and mean backscatter size via digital signal processing, *Ultrasonic Imaging 6,* 13-23 (1984).

[13] Nicolas, J., A New Method for the Analysis of the Frequency Dependence of the Backscatter Coefficient in Tissue-like Media, in *Acoustical Imaging, Vol. 14,* A. Berkout, J. Ridder and L. Van der Wal, eds., pp. 761-764 (Plenum Press, New York, 1985).

[14] Wilson, L. Robinson, D. and Doust, B., Frequency domain processing for ultrasonic attenuation measurement in liver, *Ultrasonic Imaging 6,* 278-292 (1984).

[15] Madsen,E., Insana,M., Zagzebski, J., Method of data reduction for accurate determination of ultrasonic backscatter coefficients, *J. Acoust. Soc. Am. 76,* 913-923 (1984).

[16] Morse, P.M. and Ingard, K.U., *Theoretical Acoustics*, pp. 426 (McGraw-Hill, New York, 1968).

[17] Beyer, R.T. and Letcher, S.V., *Physical Ultrasonics*, pp. 14 (Academic Press, New York, 1969).

[18] Yao, L., Reference Phantom Method For Acoustic Backscatter And Attenuation Coefficient Measurements, Ph.D. Thesis (University of Wisconsin, Madison, 1990).

[19] Harris, F., On the use of windows for harmonic analysis with the discrete Fourier transform, *Proc. IEEE 66,* 51-83 (1978).

[20] Maklad, N., Ophir, J. and Balsera, V., Attenuation of ultrasound in normal liver and diffuse liver disease *in vivo*, *Ultrasonic Imaging 6,* 117-125 (1984).

[21] Boote, E, Zagzebski, J. and Madsen, E., Backscatter coefficient imaging with a clinical scanner, Med. Phys. 19, 1145-1152 (1992).

[22] Goss, S.A., Johnston, R.L. and Dunn, F., Comprehensive compilation of empirical ultrasonic properties of mammalian tissues, *J. Acoust. Soc. Am. 64,* 423-430 (1978).

[23] Nicholas, D., Hill, C. R. and Nassiri, D. K., Evaluation of backscattering coefficients for excised human tissues: principles and techniques, *Ultrasound Med. Biol. 8,* 7-15 (1982).

[24] Bamber, J. C. and Hill, C. R., Acoustic properties of normal and cancerous liver - I. dependence of pathological conditions, *Ultrasound Med. Biol. 7,* 121-133 (1981).

[25] Yao, L., Zagzebski, J. and Madsen, E., Statistical uncertainty in ultrasonic backscatter and attenuation coefficients determined with a reference phantom, *Ultrasound Med. Biol. 17,* 197-194 (1991).

[26] Hancock, J., *An Introduction to the Principles of Communication Theory* p. 16 (McGraw-Hill, New York, 1961).